11th World Congress on Computational Mechanics (WCCM XI)
5th European Conference on Computational Mechanics (ECCM V)
6th European Conference on Computational Fluid Dynamics (ECFD VI)
E. Oñate, J. Oliver and A. Huerta (Eds)

THERMOELASTICITY IN FGM SHELL STRUCTURES

PETER A. FOTIU*, STEPHAN KUGLER* AND JUSTIN MURIN†

* Department of Applied and Numerical Mechanics,
University of Applied Sciences Wiener Neustadt, Wiener Neustadt, Austria,
kugler@fhwn.ac.at, fotiu@fhwn.ac.at and http://www.fhwn.at

† Department of Applied Mechanics and Mechatronics,
FEI, Slovak University of Technology in Bratislava, Slovakia,
justin.murin@stuba.sk and http://www.stuba.sk

Key words: Thermo-Elasticity, Shell Structures, Effective Quantities

Abstract. A thermo-elastic analysis procedure for shell structures made of functionally graded materials is proposed. The formulation is based on a general purpose quadrilateral shell element with drilling degrees of freedom, while effective elastic quantities are used in order to capture continuous or discontinuous variations of material properties within the shell's structure. Thermal expansion is included based on a weak coupling method, and the resulting solution procedure is attractive due to its efficiency since any Gaussian quadrature is avoided at element level.

1 Introduction

This paper focuses on the analysis of thermo-elastic effects in shell structures of thickness h made of functionally graded materials (FGM) or multilayer composites (MLC). The constitutive model is characterized by a variation of material properties (Young's modulus E, Poisson's ratio ν, thermal expansion coefficient α and thermal conductivity k) over the volume under consideration to achieve specific functions and applications. This variation is continuous in FGMs and discontinuous in MLCs. Here, we concentrate only on arbitrary variations of material properties in transverse direction $\hat{z}$. Variations with respect to the membrane directions $\hat{x}$, $\hat{y}$ can be modeled easily using a discretization scheme with elements each showing constant transverse variations. From a macroscopic view, a FGM is assumed to be isotropic at each material point.

Thermo-elasticity in FGM shell structures plays an important role in sensors and actuators (see eg. [1, 2, 3] and the references therein) and accurate and effective virtual analysis procedures are required. Frequently, shell like structures are combined with beam structures and the all too often missing drilling degree of freedom becomes important. This in-plane rotational degree of freedom is derived from a recently proposed functional [4],

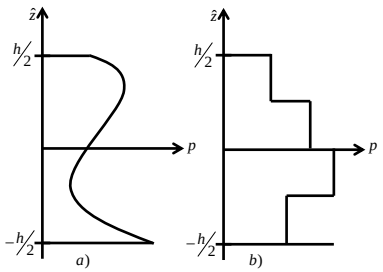

Figure 1: Variation of any material property p with respect to the transverse direction $\hat{z}$

while the corresponding six parameter shell elements are discussed in [5]. A major advantage of these low order element formulations rests on the fact that multifield variational principles enable the possibility to avoid any Gaussian quadrature at element level. All parts of the resulting stiffness matrix can be evaluated analytically leading to a gain in efficiency by a factor of four [6].

The proposed finite element requires effective elastic quantities such as the

- offset $\overline{z}$ of a neutral plane (where membrane and bending properties decouple) from a geometrical mid-plane in case of unsymmetrical variations of Young's modulus.
- effective quantities for membrane and bending deformations E_m and E_b.
- shear correction factor α_s in case of first order shear elastic bending theories.

A detailed derivation is discussed in [7] and in the references therein and will not be repeated here. Instead, this paper is focused on the analytical description of thermo-elastic properties. In most FGM applications Poisson's ratio does not vary substantially. Hence, ν is assumed to be constant within an element.

The paper is organized as follows: In Sect. 2 the derivation of effective elastic quantities is shortly discussed, while new results for power-law distributions are presented. In Sect. 3 the effects of thermal expansion are introduced, and the resulting formulation is tested in Sect. 4 based on some benchmark problems.

2 Effective elastic quantities

The element formulation requires four effective quantities that are directly related to the distribution of Young's modulus $E(\hat{z})$, see Fig. 1 with $p = E$. In case of unsymmetrical variations of E the offset $\overline{z}$ of a neutral surface from the discretized mid-plane is evaluated as

$$\overline{z} = \frac{\int_{-h/2}^{h/2} E(\hat{z})\hat{z}d\hat{z}}{\int_{-h/2}^{h/2} E(\hat{z})d\hat{z}}. \tag{1}$$

With respect to this neutral surface membrane and bending deformations are decoupled and an arbitrary normal strain distribution $\varepsilon(\hat{z}')$ reads

$$\varepsilon(\hat{z}') = \varkappa \hat{z}' + \varepsilon_0, \tag{2}$$

with $\hat{z}' = \hat{z} - \overline{z}$. In (2) ε_0 denotes the strain in the mechanical neutral surface, while $\varkappa$ is the curvature[1]. The effective moduli for membrane (E_m) and bending (E_b) read

$$E_m = \frac{1}{h} \int\limits_{-h/2-\overline{z}}^{h/2-\overline{z}} E(\hat{z}') d\hat{z}', \tag{3}$$

$$E_b = \frac{12}{h^3} \int\limits_{-h/2-\overline{z}}^{h/2-\overline{z}} E(\hat{z}') \hat{z}'^2 d\hat{z}'. \tag{4}$$

For shear elastic shell formulations the shear correction factor α_s is given by

$$\frac{1}{\alpha_s} = \frac{144}{E_b h^5} \int\limits_{-h/2-\overline{z}}^{h/2-\overline{z}} \frac{1}{E(\hat{z}')} \left[\int\limits_{\hat{z}'}^{h/2-\overline{z}} E(\zeta) \zeta d\zeta \right]^2 d\hat{z}', \tag{5}$$

and the shear stiffness reads

$$\frac{E_b \alpha_s h}{2(1+\nu)}. \tag{6}$$

In the following we evaluate the effective elastic quantities for a power-law distribution, which is most commonly adopted in FGM formulations. Young's modulus varies according to ,

$$E(\hat{z}) = (E_2 - E_1) \left(\frac{2\hat{z}/h + 1}{2} \right)^n + E_1, \tag{7}$$

with E_1 and E_2 denoting the moduli at $\hat{z} = -h/2$ and $\hat{z} = h/2$. The power-law exponent n indicates the profile of the variation with respect to the thickness direction with

$$k = E_2/E_1. \tag{8}$$

Fig. 2 depicts the distribution of $E(\hat{z})$ for several exponents n and $k = 10$. The effective elastic constants ($\overline{z}$, E_m, E_b and α_s) can be evaluated from (7) and are displayed in Fig. 3 with respect to n. The analytical form of $\overline{z}$ reads

$$\overline{z} = \frac{h(k-1)n(n+1)}{2(k+n)(2+3n+n^2)}. \tag{9}$$

[1]Here, $\varepsilon(\hat{z}')$ is representative for any normal strain, i.e. $\varepsilon_{\hat{x}\hat{x}}$ and $\varepsilon_{\hat{y}\hat{y}}$, respectively, while the curvature $\varkappa$ stands for the curvatures $\varkappa_{\hat{x}}$ and $\varkappa_{\hat{y}}$.

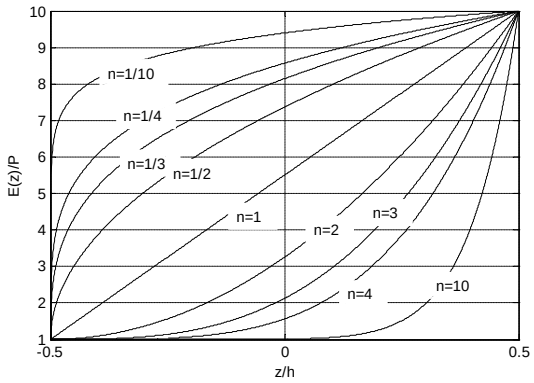

Figure 2: Effect of the power-law exponent n on the Young's modulus distribution with $k = 10$

and the effective moduli for membrane and bending properties are independent of h

$$E_m = \frac{E_1(k+n)}{n+1}, \tag{10}$$

$$E_b = \frac{E_1(12k^2 + 4kn(7+n(n+4)) + n^2(7+n(n+4)))}{(n+2)^2(n+3)(k+n)}. \tag{11}$$

An analytical representation of the shear correction factor α_s is not easily accessible, and can be conveniently estimated from graphical representations in Fig. 3.

3 Weak coupling of thermal expansion

The finite element formulation discussed in [7] is based on a weak form of the equilibrium conditions, which read in the absence of external loads

$$\delta\Pi = \int (\delta\boldsymbol{\varepsilon})^T \boldsymbol{\sigma} dV = 0. \tag{12}$$

Equation (12) depicts the virtual internal work $\delta\Pi$ in one finite element of volume V, where we omitted any external loads. The stress and virtual strain tensor in matrix notation is denoted by $\boldsymbol{\sigma}$ and $\delta\boldsymbol{\varepsilon}$. The constitutive equations read

$$\varepsilon_{\hat{x}\hat{x}} = \frac{1}{E(\hat{z})}(\sigma_{\hat{x}\hat{x}} - \nu\sigma_{\hat{y}\hat{y}}) + \alpha(\hat{z})\Delta T(\hat{z}),$$

$$\varepsilon_{\hat{y}\hat{y}} = \frac{1}{E(\hat{z})}(\sigma_{\hat{y}\hat{y}} - \nu\sigma_{\hat{x}\hat{x}}) + \alpha(\hat{z})\Delta T(\hat{z}),$$

$$\varepsilon_{\hat{z}\hat{z}} = \frac{-\nu}{E(\hat{z})}(\sigma_{\hat{x}\hat{x}} + \sigma_{\hat{y}\hat{y}}) + \alpha(\hat{z})\Delta T(\hat{z}),$$

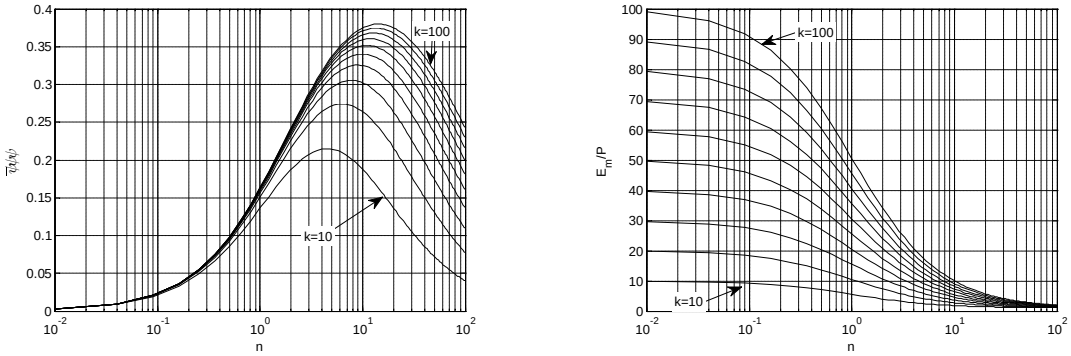

(a) Offset of neutral plane $\overline{z}$

(b) Effective membrane module E_m

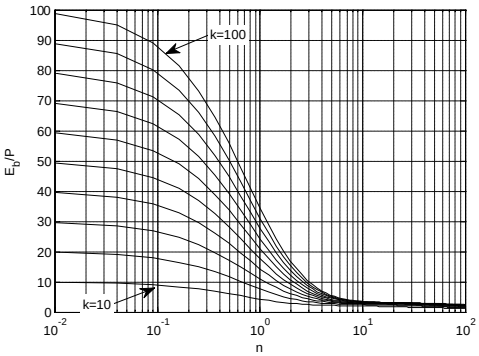

(c) Effective bending module E_b

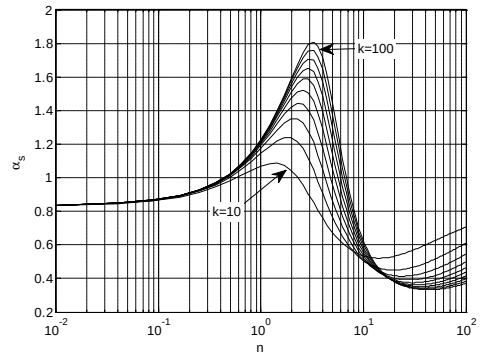

(d) Shear correction factor α_s

Figure 3: Effective elastic quantities with respect to power-law exponent n and k =10, 20, 30, 40, 50, 60, 70, 80, 90, 100

$$\gamma_{\hat{x}\hat{y}} = \frac{2(1+\nu)}{E(\hat{z})}\sigma_{\hat{x}\hat{y}}, \tag{13}$$

where we adopted a plane stress constraint, i.e. $\sigma_{\hat{z}\hat{z}} = 0$. The thermal expansion coefficient $\alpha(\hat{z})$ shows an arbitrary variation with respect to $\hat{z}$ (see Fig. 1). The temperature distribution $\Delta T(\hat{z})$ is based on a thermal conduction problem with arbitrary variations of thermal conductivity and independent convection boundary conditions at the top and bottom surface. An iterative solution procedure for this problem is given in [8]. From (13) we obtain the stresses

$$\begin{aligned}
\sigma_{\hat{x}\hat{x}} &= \frac{E(\hat{z})}{1-\nu^2}(\varepsilon_{\hat{x}\hat{x}} + \nu\varepsilon_{\hat{y}\hat{y}}) - \frac{E(\hat{z})\alpha(\hat{z})\Delta T(\hat{z})}{1-\nu}, \\
\sigma_{\hat{y}\hat{y}} &= \frac{E(\hat{z})}{1-\nu^2}(\varepsilon_{\hat{y}\hat{y}} + \nu\varepsilon_{\hat{x}\hat{x}}) - \frac{E(\hat{z})\alpha(\hat{z})\Delta T(\hat{z})}{1-\nu}, \\
\sigma_{\hat{x}\hat{y}} &= \frac{E(\hat{z})}{2(1+\nu)}\gamma_{\hat{x}\hat{y}},
\end{aligned} \tag{14}$$

or in matrix notation

$$\begin{bmatrix} \sigma_{\hat{x}\hat{x}} \\ \sigma_{\hat{y}\hat{y}} \\ \sigma_{\hat{x}\hat{y}} \end{bmatrix} = \frac{E(\hat{z})}{1-\nu^2} \begin{bmatrix} 1 & \nu & 0 \\ \nu & 1 & 0 \\ 0 & 0 & \frac{1-\nu}{2} \end{bmatrix} \begin{bmatrix} \varepsilon_{\hat{x}\hat{x}} \\ \varepsilon_{\hat{y}\hat{y}} \\ \varepsilon_{\hat{x}\hat{y}} \end{bmatrix} - \frac{E(\hat{z})\alpha(\hat{z})\Delta T(\hat{z})}{1-\nu} \begin{bmatrix} 1 \\ 1 \\ 0 \end{bmatrix},$$

$$\boldsymbol{\sigma} = \mathbf{C}\boldsymbol{\varepsilon} - \frac{E(\hat{z})\alpha(\hat{z})\Delta T(\hat{z})}{1-\nu} \begin{bmatrix} 1 \\ 1 \\ 0 \end{bmatrix}. \tag{15}$$

We insert (15) into (12)

$$\delta\Pi = \delta\Pi_m - \delta\Pi_t = \int\limits_{V_e} (\delta\boldsymbol{\varepsilon})^T \mathbf{C}\boldsymbol{\varepsilon} dV - \int\limits_{V_e} (\delta\boldsymbol{\varepsilon})^T \frac{E(\hat{z})\alpha(\hat{z})\Delta T(\hat{z})}{1-\nu} \begin{bmatrix} 1 \\ 1 \\ 0 \end{bmatrix} dV = 0, \tag{16}$$

where the first term on the RHS is devoted to the element stiffness matrix, while the second part refers to internal forces and couples caused by thermal loading. In connection with (16) we get

$$\delta\Pi_t = \int\limits_{V_e} \begin{bmatrix} \delta\varepsilon_{\hat{x}\hat{x}} & \delta\varepsilon_{\hat{y}\hat{y}} \end{bmatrix} \frac{E(\hat{z})\alpha(\hat{z})\Delta T(\hat{z})}{1-\nu} \begin{bmatrix} 1 \\ 1 \end{bmatrix} dV, \tag{17}$$

where the virtual normal-strain field is related to displacements and rotations, i.e.

$$\begin{bmatrix} \delta\varepsilon_{\hat{x}\hat{x}} & \delta\varepsilon_{\hat{y}\hat{y}} \end{bmatrix} = \begin{bmatrix} \delta u_{\hat{x},\hat{x}} + \hat{z}\varphi_{\hat{y},\hat{x}} & \delta u_{\hat{y},\hat{y}} - \hat{z}\varphi_{\hat{x},\hat{y}} \end{bmatrix}. \tag{18}$$

Interpolating the displacement and rotation field with classical bilinear shape-functions $\mathbf{N}$,

$$\begin{bmatrix} u_{\hat{x}} \\ u_{\hat{y}} \end{bmatrix} = \begin{bmatrix} \mathbf{N} & \mathbf{0} \\ \mathbf{0} & \mathbf{N} \end{bmatrix} \begin{bmatrix} \mathbf{U}_{\hat{x}} \\ \mathbf{U}_{\hat{y}} \end{bmatrix} \quad \text{and} \quad \begin{bmatrix} \varphi_{\hat{x}} \\ \varphi_{\hat{y}} \end{bmatrix} = \begin{bmatrix} \mathbf{N} & \mathbf{0} \\ \mathbf{0} & \mathbf{N} \end{bmatrix} \begin{bmatrix} \boldsymbol{\Phi}_{\hat{x}} \\ \boldsymbol{\Phi}_{\hat{y}} \end{bmatrix}, \tag{19}$$

leads to

$$\delta\Pi_t = \begin{bmatrix} \delta\mathbf{U}_{\hat{x}}^T & \delta\mathbf{U}_{\hat{y}}^T \end{bmatrix} \begin{bmatrix} \mathbf{F}_{\hat{x}} \\ \mathbf{F}_{\hat{y}} \end{bmatrix} + \begin{bmatrix} \delta\boldsymbol{\Phi}_{\hat{x}}^T & \delta\boldsymbol{\Phi}_{\hat{y}}^T \end{bmatrix} \begin{bmatrix} \mathbf{M}_{\hat{x}} \\ \mathbf{M}_{\hat{y}} \end{bmatrix}, \tag{20}$$

with

$$\mathbf{F}_{\hat{x}} = \int\limits_{V_e} \mathbf{N}_{,\hat{x}} \frac{E(\hat{z})\alpha(\hat{z})\Delta T(\hat{z})}{1-\nu} dV \quad , \quad \mathbf{F}_{\hat{y}} = \int\limits_{V_e} \mathbf{N}_{,\hat{y}} \frac{E(\hat{z})\alpha(\hat{z})\Delta T(\hat{z})}{1-\nu} dV,$$

$$\mathbf{M}_{\hat{x}} = -\int\limits_{V_e} \mathbf{N}_{,\hat{y}} \hat{z} \frac{E(\hat{z})\alpha(\hat{z})\Delta T(\hat{z})}{1-\nu} dV \quad , \quad \mathbf{M}_{\hat{y}} = \int\limits_{V_e} \mathbf{N}_{,\hat{x}} \hat{z} \frac{E(\hat{z})\alpha(\hat{z})\Delta T(\hat{z})}{1-\nu} dV. \tag{21}$$

Note that differentiating the shape functions with respect to $\hat{x}$ and $\hat{y}$ leads to a factor $1/\det\mathbf{J}$ ($\mathbf{J}$ being the Jacobian matrix), while dV is proportional to $\det\mathbf{J}$. Hence, they

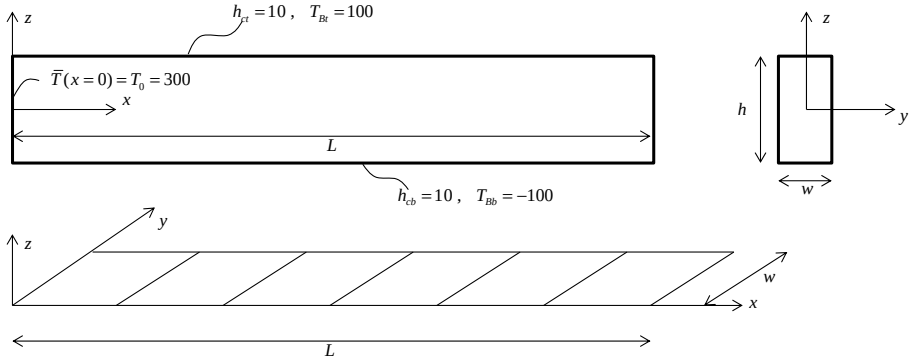

Figure 4: Thick thermo-elastic FGM-fin

cancel each other leaving the integrands as pure polynomials. They can be integrated analytically, if the distributions of E, α and ΔT are assumed to be constant throughout the element's area. With the bilinear shape functions $\mathbf{N}$ we obtain from (21)

$$\mathbf{F}_{\hat{x}} = \frac{1}{2}\begin{bmatrix} \hat{y}_{24} \\ \hat{y}_{31} \\ \hat{y}_{42} \\ \hat{y}_{13} \end{bmatrix} \int_{-h/2}^{h/2} \frac{E(\hat{z})\alpha(\hat{z})\Delta T(\hat{z})}{1-\nu} d\hat{z} \quad , \quad \mathbf{F}_{\hat{y}} = \frac{1}{2}\begin{bmatrix} \hat{x}_{42} \\ \hat{x}_{13} \\ \hat{x}_{24} \\ \hat{x}_{31} \end{bmatrix} \int_{-h/2}^{h/2} \frac{E(\hat{z})\alpha(\hat{z})\Delta T(\hat{z})}{1-\nu} d\hat{z},$$

$$\mathbf{M}_{\hat{x}} = \frac{1}{2}\begin{bmatrix} \hat{x}_{24} \\ \hat{x}_{31} \\ \hat{x}_{42} \\ \hat{x}_{13} \end{bmatrix} \int_{-h/2}^{h/2} \hat{z}\frac{E(\hat{z})\alpha(\hat{z})\Delta T(\hat{z})}{1-\nu} d\hat{z} \quad , \quad \mathbf{M}_{\hat{y}} = \frac{1}{2}\begin{bmatrix} \hat{y}_{24} \\ \hat{y}_{31} \\ \hat{y}_{42} \\ \hat{y}_{13} \end{bmatrix} \int_{-h/2}^{h/2} \hat{z}\frac{E(\hat{z})\alpha(\hat{z})\Delta T(\hat{z})}{1-\nu} d\hat{z}. \tag{22}$$

These elemental forces and couples refer to the discretized mid-surface and have to be transformed to the neutral surface.

4 Numerical examples

In this section two challenging benchmark problems are introduced. The temperature distributions in membrane and transverse direction are evaluated using the solution procedure proposed in [8]. The resulting temperature and displacement fields are compared to continuum solutions with the aid of ANSYS.

4.1 Thick thermo-elastic FGM fin

Consider a thick FGM structure depicted in Fig. 4 ($L = 10$, $h = 2$, $w = 1$) which is subjected to a convection boundary condition (convection coefficients h_c and fluid temperature T_B) on the top and bottom surface, respectively, i.e. $h_{ct} = 10$, $T_{Bt} = 100$ and $h_{cb} = 10$, $T_{Bb} = -100$. The mean temperature is prescribed at $x = 0$ via $\overline{T}(x = 0, y) = 300$ and the geometrical mid-surface is discretized with N elements. The left end at $x = 0$ is

	Configuration 1	Configuration 2
Thermal conductivity	$k(z) = 50z + 51$	$k(z) = 50z + 51$
Young's modulus	$E(z) = 10$	$E(z) = -9z + 10$
Poisson's ratio	$\nu = 0$	$\nu = 0$
Thermal expansion coefficient	$\alpha(z) = 1 \cdot 10^{-4}$	$\alpha(z) = 0.9 \cdot 10^{-4} + 1 \cdot 10^{-4}$

Table 1: Material properties of thick thermo-elastic FGM-fin

clamped, and the material properties are given in Tab. 1 where two configurations are introduced. Both configurations show the same linearly distributed thermal conductivity. Configuration 1 has a constant Young's modulus and a constant thermal conductivity and deformations through thermo-elasticty occur only due to evaluated temperature distributions. Configuration 2 is a functionally graded material where all relevant quantities are linearly distributed. Without loss of generality Poisson's ratio is assumed zero.

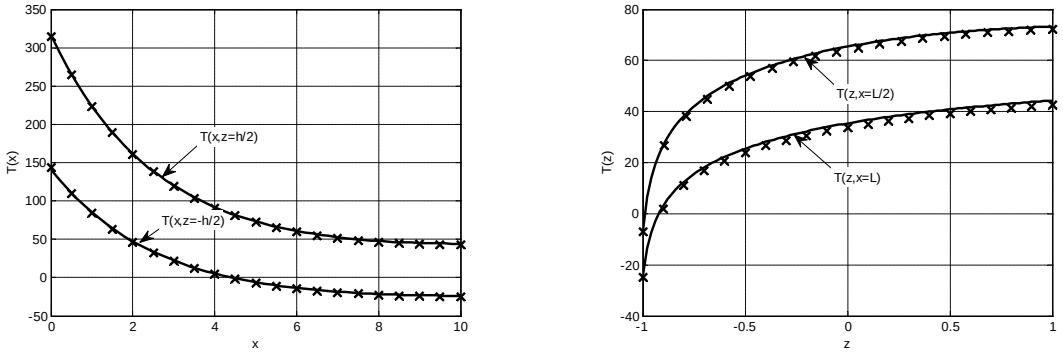

(a) Temperature distribution on top and bottom surface

(b) Temperature distribution in transverse direction

Figure 5: Temperature distributions in thick FGM fin

The reference solutions are found from a fully coupled (non-linear) Plane 13 element in ANSYS where a discretization of 500×190 elements is used. The mean temperature at the left end is prescribed by applying a von Neumann boundary condition in the ANSYS solution, i.e.

$$q_n(x = 0,\, z) = -113.4028k(z). \tag{23}$$

The temperature distributions at the top and bottom surface are depicted in Fig. 5a, and the distributions with respect to the transverse direction are shown in Fig. 5b at $x = {}^{L}/_{2}$ and $x = L$. The solid lines correspond to the present solution procedure with $N = 50$ while the asterisks refer to the ANSYS solution. We observe good accuracy compared to the ANSYS solution, and we see that the temperature field varies strongly in the FGM structure. Based on these temperature variations the displacements are evaluated

		Configuration 1	Configuration 2
Present	u_x	0.0913	0.0987
	u_z	-0.1433	-0.6782
ANSYS	u_x	0.0903	0.0972
	u_z	-0.1428	-0.6746

Table 2: Displacement at $x = L$ and $z = 0$

at $x = L$ and $z = 0$ for both configurations and compared to ANSYS (see Tab. 2). A relative error of less than two percent is found regardless of the discretization scheme. This is due to the completely different solution procedure in ANSYS where a fully coupled thermo-elastic solution is performed. Nevertheless, the proposed algorithm is accurate in this challenging problem.

4.2 FGM shell structure

Consider the hemisphere of Fig. 6a with a radius $R = 10$ and a thickness of $h = 0.5$. Due to symmetry only on quarter of the structure is regularly meshed with N arbitrarily shaped and warped shell elements (Fig. 6b). The material properties and boundary conditions depend only on a radial coordinate r, thus, only one quarter of the structure will be analyzed[2]. The model is loaded at the inner and outer surface with a convection boundary condition,

$$h_{ct} = h_{cb} = 10 \ , \ \ T_{Bt} = 0 \ , \ \ T_{Bb} = 300, \tag{24}$$

and at the equator the mean temperature is kept at $\overline{T} = 500$. Due to these thermal

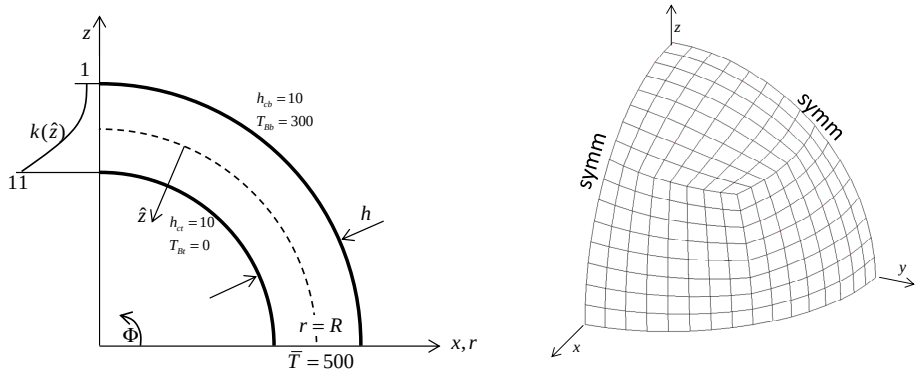

(a) FGM shell structure (b) Shell mesh: $N = 192$

Figure 6: Problem description - FGM shell structure

[2]This axisymmetric problem could be analyzed with less than a quarter, however, in order to check the performance of the proposed formulation regarding warped element configurations, we use one quarter of the structure.

boundary conditions we expect strong variations of temperature in thickness direction $\hat{z}$ and in membrane direction ϕ. The material parameters show only variations of the thermal conductivity,

$$k(\hat{z}) = 3.5 + 20\hat{z} + 40\hat{z}^2, \tag{25}$$

representing a parabolic distribution with low conductivity at the outside, $k(\hat{z} = -h/2) = 1$, and high conductivity at the inner surface, $k(\hat{z} = h/2) = 11$. Young's modulus E,

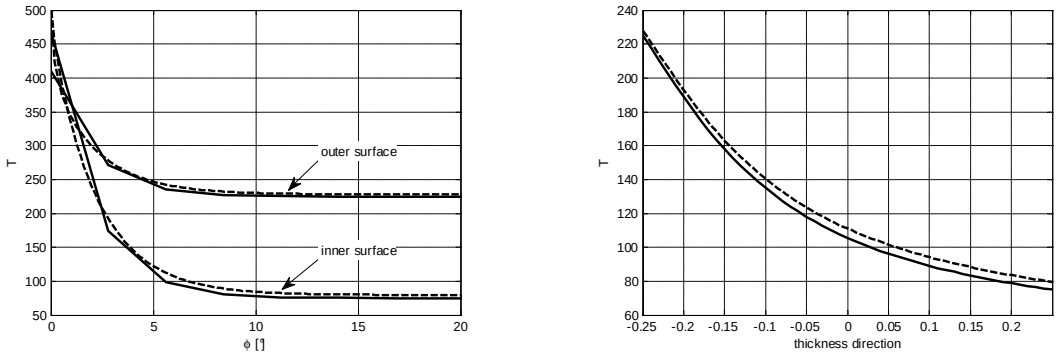

(a) Temperature distribution along the meridian

(b) Temperature distribution with respect to $\hat{z}$ at $\phi = 90$

Figure 7: Temperature distributions in FGM shell structure (Solid line: Present formulation, Dashed line: ANSYS) - $N = 768$, $n = 50$, $I = 10$

Poisson's ratio ν and thermal expansion α are constant with respect to the thickness direction in order to clearly see the influence of temperature variations, i.e.

$$E = 10 \ , \ \ \nu = 0.3 \ , \ \ \alpha = 1 \cdot 10^{-4}. \tag{26}$$

Note that the performance of the proposed formulation regarding pure elasticity solutions of an FGM hemisphere with a varying Young's modulus can be found in [9]. The reference results are evaluated using an axisymmetric model in ANSYS with the fully coupled Plane 13 element and a very fine discretization of 100×500. For sake of convenience we apply a thermal Dirichlet boundary condition of $T(R - h/2 \leq x \leq R + h/2) = 500$ accepting some error discussed in [8]. A detail of the temperature distributions with respect to the meridian $0 \leq \phi \leq 90$ is shown in Fig. 7a. Due to high convection coefficients $h_{cb} = h_{ct} = 10$ the temperature does not show any variations for $\phi > 20$. The temperature field with respect to the thickness direction is depicted in Fig. 7b. The distributions evaluated with the present formulation (solid lines) are compared to the ANSYS solutions (dashed lines), indicating good accuracy. The displacements in radial direction u_r and in height direction u_z due to thermal expansion are listed in Tab. 3 for different numbers of shell elements. We observe convergence with respect to N for displacements in radial direction leading to very accurate results for $N = 768$. In terms of displacements in height direction some error of $< 4\%$ has to be accepted.

	u_r	u_z	error in u_r	error in u_z
ANSYS	0.2104	-0.1256	-	-
present $N = 48$ elements	0.2646	-0.1216	25.7%	3.2%
present $N = 192$ elements	0.2261	-0.1211	7.5%	3.6%
present $N = 768$ elements	0.2100	-0.1210	0.2%	3.7%

Table 3: Displacements of FGM shell structure

5 Conclusion

In this paper a very efficient solution strategy of thermo-elastic problems of shell structures made of functionally graded materials is proposed. The resulting numerical framework is based on a low order shell formulation with drilling degrees of freedom. There, any Gaussian quadrature is avoided since all parts of the stiffness matrix can be integrated analytically. The shell formulation requires effective elastic quantities as the offset of the neutrals surface, the effective moduli for membrane and bending properties and the shear correction factor. Detailed formulas describing those quantities are given and are evaluated for the frequently used power-law representation of a Young's modulus distribution with respect to the thickness direction. Thermo-elastic effects are included based on a weak coupling. The resulting internal forces and moments can again be evaluated without any numerical integration in membrane direction. The resulting formulation is tested within two benchmark problems, all indicating accurate predictive quality.

Acknowledgment:

This paper has been supported by Grant Agency VEGA - Project Number: 1/0534/12, and by APVV-0246-12.

REFERENCES

[1] S. Chakraborty, S. Gopalakrishnan, J. Reddy, A new beam finite element for the analysis of functionally graded materials, *International Journal of Mechanical Sciences* 45 (2003) 519–539.

[2] A. Mahi, E. A. Bedia, A. Tounsi, I. Mechab, An analytical method for temperature-dependent free vibration analysis of functionally graded beams with general boundary condition, *Composite Structures* 92 (2010) 1877–1887.

[3] R. Naghdabadi, S. H. Kordkheili, A finite element formulation for analysis of functionally graded plates and shells, *Archive of applied mechanics* 74 (2005) 375–386.

[4] S. Kugler, P. Fotiu, J. Murin, A highly efficient membrane finite element with drilling degrees of freedom, *Acta Mechanica* 213 (2010) 323–348.

[5] S. Kugler, P. Fotiu, J. Murin, Advances in quadrilateral shell elements with drilling degrees of freedom, *EUROMECH Colloquium 527* Shell-like Structures: Nonclassical Theories and Applications.

[6] S. Kugler, Development of a laterally pressed quadrilateral shell element, Ph.D. thesis, STU Bratislava (2010).

[7] S. Kugler, P. Fotiu, J. Murin, The numerical analysis of fgm shells with enhanced finite elements, *Engineering Structures* 49 (2013) 920–935.

[8] S. Kugler, P.A.Fotiu, J. Murin, Thermal conduction in FGM and MLC shell structures, Proceeding at 11th World Congress on Computational Mechanics (WCCM XI) in Barcelona.

[9] S. Kugler, P. Fotiu, J. Murin, Enhanced functionally graded material shell finite elements, *ZAMM Z. Angew. Math. Mech.* (2013) 1–13.